Two-dimensional carrier density distribution inside a high power tapered laser diode

R. Pagano' , M. Ziegler, J. W. Tomm, I. Esquivias, J. M. G. Tijero, J. R. O'Callaghan, N. Michel, M. Krakowski, and B. Corbett

Citation: Appl. Phys. Lett. **98**, 221110 (2011); doi: 10.1063/1.3596445
View online: http://dx.doi.org/10.1063/1.3596445
View Table of Contents: http://aip.scitation.org/toc/apl/98/22
Published by the American Institute of Physics

Two-dimensional carrier density distribution inside a high power tapered laser diode

R. Pagano,[1,a)] M. Ziegler,[2] J. W. Tomm,[3] I. Esquivias,[4] J. M. G. Tijero,[4] J. R. O'Callaghan,[1] N. Michel,[5] M. Krakowski,[5] and B. Corbett[1]
[1]*Tyndall National Institute, University College Cork, Lee Maltings, Cork, Ireland*
[2]*BAM Federal Institute for Materials Research and Testing, 12200 Berlin, Germany*
[3]*Max Born Institut, Berlin, Germany*
[4]*E. T. S. I. de Telecomunicación, Universidad Politécnica de Madrid, 28040 Madrid, Spain*
[5]*Alcatel-Thales III-V Lab, 91767 Palaiseau, France*

(Received 11 February 2011; accepted 10 May 2011; published online 3 June 2011)

The spontaneous emission of a GaAs-based tapered laser diode emitting at $\lambda = 1060$ nm was measured through a window in the transparent substrate in order to study the carrier density distribution inside the device. It is shown that the tapered geometry is responsible for nonuniform amplification of the spontaneous/stimulated emission which in turn influences the spatial distribution of the carriers starting from below threshold. The carrier density does not clamp at the lasing threshold and above it the device shows lateral spatial hole-burning caused by high stimulated emission along the cavity center. © *2011 American Institute of Physics*. [doi:10.1063/1.3596445]

Tapered semiconductor lasers, originally proposed by Walpole *et al.*[1,2] and with recent advances in their performance[3,4] and design,[5] represent an efficient, cheap, and compact solution to achieve high brightness and reliability due to their high threshold for catastrophic optical mirror damage. The tapered cavity, shown in Fig. 1, consists of a ridge waveguide (RW) section that works as filter against high order lateral modes and a gain-guided tapered section that amplifies the optical mode and allows its smooth diffraction from the ridge. Spontaneous emission (SE) measurements[6] are of great interest to map the carrier density in this quasi-two-dimensional cavity system so as to understand the factors that influence the ultimate beam quality. A nonuniform distribution of carriers inside a tapered laser will result in spatially nonuniform index variations, which cause a degradation of beam quality and ultimately lead to beam filamentation and/or device failure.

In this letter, we show that in tapered lasers the SE is spatially not uniform even below the laser threshold. At a fixed current, the SE increases from the ridge section toward the output of the taper, until it reaches a maximum and then diminishes monotonically to the device facet. The nonuniformity of SE was reported for Fabry–Pérot lasers but just above threshold[7] and for semiconductor optical amplifiers above the transparency.[8] To the best of our knowledge, experimental[9] and theoretical[10] analysis of the carrier distribution inside tapered cavities have been already carried on but only considering the devices in operation above threshold. In the experimental work of Ref. 9, however, the carrier distribution was analyzed only in the lateral direction.

The sample investigated is based on an InGaAs single-quantum well (SQW) emitting around 1060 nm as active region surrounded by a GaInAsP waveguide and AlGaAs cladding layers.[11] The structure was grown by metal-organic vapor phase epitaxy on an *n*-type GaAs substrate. The device is an unstable resonator providing a theoretical magnification $M \approx 210$,[12] consisting of a 1 mm long, 3 μm wide, and 1.8 μm high RW and a gain-guided tapered region, 3 mm long with a full angle of 6° with an input aperture as the ridge width and an output width of 314 μm. The large output facet of the taper is low-reflectivity coated ($5\% < R < 10\%$, where R is the power reflectivity) while the rear facet is high-reflectivity coated ($70\% < R < 80\%$). The laser was mounted *p*-side down on a water-cooled heat-sink with the temperature kept stable at 23 ± 0.02 °C. A window opened in the metallization on the *n*-type substrate of the device permitted the collection of the light emitted through the transparent GaAs substrate with a 5× microscope lens and a silicon charge coupled device (CCD) camera. The nominal optical resolution was 1.38 μm. Due to a limit on the field of view in the CCD the sample was imaged (see Fig. 2) from $z=0$ (output facet of the taper) to $z=2.75$ mm (close to the start of the taper). The device was tested in quasi-cw regime as rectangular waveform (repetition rate $f=1$ kHz) was used to supply the device. The duty cycle was reduced from 95% and 15% to keep the pulse shape rectangular with the current and to avoid the camera saturation with the increasing current. The intensity data were rescaled according to the pulse duty cycle and the integration times used for each value of current. The rescaling was tested by measuring the SE intensity with a multimode optical fiber along the

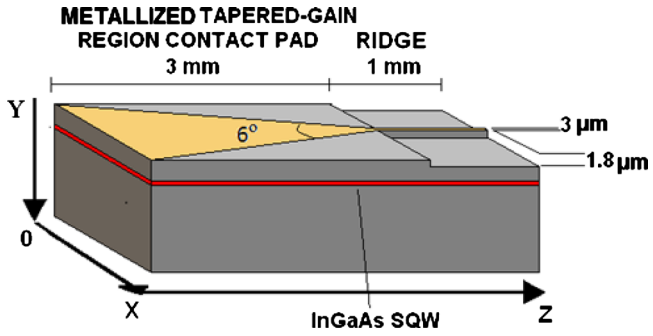

FIG. 1. (Color online) Schematic diagram of the tapered laser investigated and the reference system used.

a)Electronic mail: roberto.pagano@tyndall.ie.

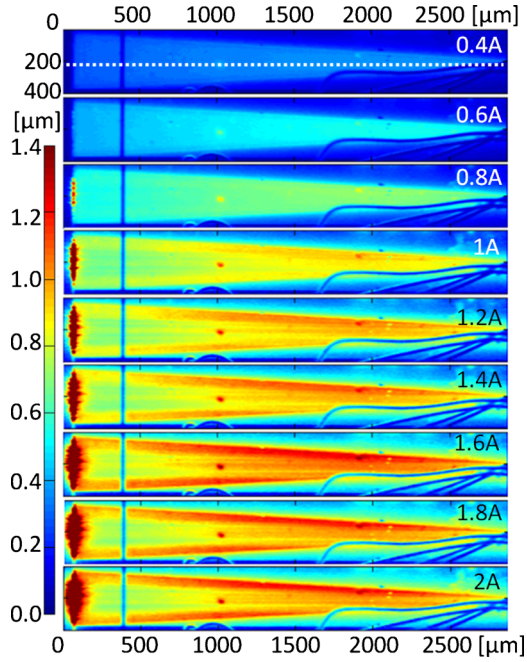

FIG. 2. (Color online) SE intensity maps for different currents (0.4–2 A) concentrating on the flared region in order to maintain a high spatial resolution. The dotted white line (0.4 A) indicates the resonator axis. The SE is not uniform below threshold (I_{th}=750 mA) with a maximum close to the narrow taper section. Above threshold, the onset of the lateral hole burning is indicated by a nonuniform carrier depletion by the stimulated emission. The blue curved lines are bonding wires partly crossing the device while vertical dark line at $z \approx 0.4$ mm is due to a metal stripe in the *n*-substrate.

resonator axis in cw obtaining the same characteristics as in quasi-cw regime.

The SE intensity, I_{SE}, is proportional to the square of the local carrier density with a good approximation.[13] The two-dimensional SE maps measured through the substrate of the device are shown in Fig. 2 for different current values starting from below threshold (I_{th}=750 mA and J_{th} =155 A/cm^2) to almost three times I_{th}. When the current is increased above threshold the lateral uniformity of the of the SE is perturbed and we observe the formation of two intense lateral side lobes at the edge of the contact that are indicative of the onset of spatial hole-burning in the center of the device [see details in Figs. 3(a) and 3(b)]. Below threshold the SE decreases monotonically to the output facet (z=0 mm) while above threshold it reaches a local maximum around $z \sim 2$ mm the location of which changes with the injection level [see details in Fig. 3(c)]. The apparent higher intensity near the output facet (z=0) is an artefact due to the scattered stimulated emission. The integrals of the SE along the lateral direction, shown in Fig. 3(d), decrease monotonically with longitudinal position below threshold being proportional to the carriers injected while above threshold a drop in the intensity is observed close to the output because more carriers are recombined by the stimulated emission (S_tE).

The longitudinally nonuniform SE intensity distribution is a consequence of the spatially dependent amplified SE (ASE), below threshold, and of the S_tE above it. The I_{SE}, can be then expressed as the difference between the total optical intensity generated in the cavity (spontaneous+stimulated emission), I_{TOT}, and the ASE/S_tE intensity,

$$I_{SE}(J,z) = I_{TOT}(J) - \frac{P(J,z=0)}{[dW_R + 2d(L_T - z)\tan(\phi)]} \times \left\{ \exp\left\{ \left[\Gamma g \ln\left(\frac{J}{J_T}\right) - \alpha_{INT} \right](L_T - z) \right\} + R_F \exp\left\{ \left[\Gamma g \ln\left(\frac{J}{J_T}\right) - \alpha_{INT} \right] z \right\} \right\}, \quad (1)$$

where J is the injected current density considered spatially uniform, J_T is the transparency current density, $P(J,z)$ is the power at the z position, measured in W, of the ASE (below threshold) or of the S_tE (above threshold), d is the thickness of the quantum well, ϕ is the taper half angle of aperture, W_R is the ridge width, L_T is the length of the taper, R_F is the front mirror reflectivity, g is the gain coefficient, Γ is the confinement factor inside the active region, and α_{INT} quantifies the internal losses (scattering+reabsorption). Equation (1) essentially expresses the ASE/S_tE intensity as the ration of an exponentially growing power divided by a linearly growing

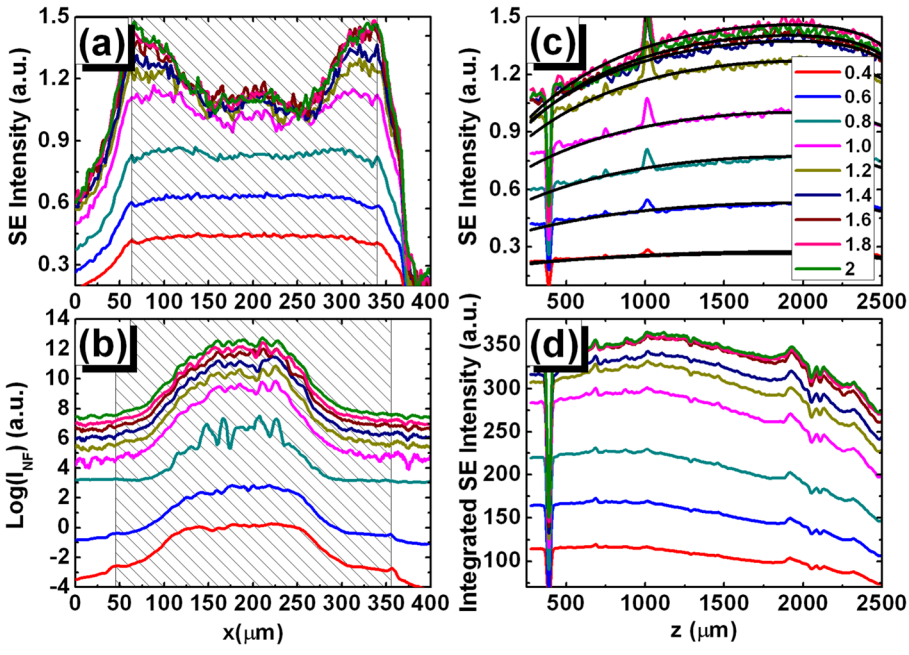

FIG. 3. (Color online) (a) Lateral SE intensity distributions at the position z=500 μm from the output facet for different currents starting from below threshold. The shaded area indicates the stripe width while the legend in the picture (b) is valid for (a), (c), and (d) too. (b) Logarithm of the near field intensity as function of current reimaged with a 4 mm focal distance lens with 0.5 numerical aperture. (c) SE intensity along the resonator axis (see white dotted line in Fig. 2) for positions from 250 μm$<z<$2500 μm for different current values. The black curves indicate the fits obtained by applying Eq. (1). The drop at z=400 μm and the peak at 1000 μm in the intensity are due to an obscuring metal line on the substrate and to a scattering defect in the substrate, respectively. (d) Integrated SE intensity along the lateral as function of z. Above threshold the S_tE reduces the SE intensity close to the output facet due to the high carriers recombination rate. The perturbations of the curves in the range 1750 μm $<z<$2150 μm are due to partial obscuration by the bonding wires.

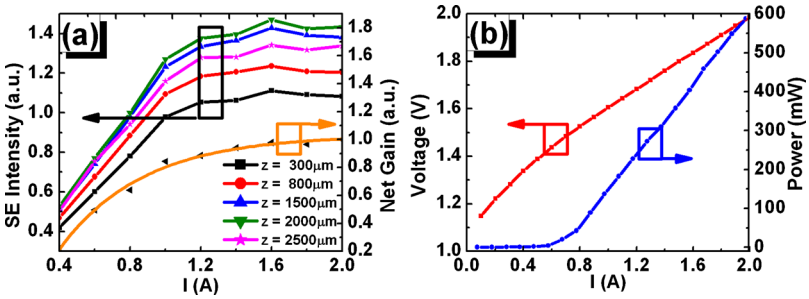

FIG. 4. (Color online) (a) SE intensity as function of the current for different positions along the resonator axis and net gain (left triangles) calculated by fitting the SE curves of Fig. 3(c). A logarithmic fit to the net gain is shown (solid line). The carrier density clamping takes place around 1.2 A compared with a threshold current of 0.75 A and is similar for all the points along the axis. (b) Voltage/power vs current characteristic showing a linear behavior above threshold with a small kink between $I=1.2$ A and $I=1.4$ A. The slope efficiency is 0.43 W/A.

cross-section. Below threshold even if the gain is not enough to overcome the round trip losses, it can still overcome the internal losses and influence the carrier density distribution on an optical path whose length is less than the round trip. The tapered cavity can be approximated to a single pass amplifier where the reflected portion of the beam at the output facet is not enough to sustain itself in the backward propagation because of the combined effect of the front facet mirror loss and geometrical losses in the backward direction. The carriers are more efficiently depleted close to the output facet and the SE intensity decreases monotonically from the narrow input to the large taper facet. Above threshold, the sum of the forward and backward optical field is maximized close to the narrow input of the taper which result in a decrease in the SE here ($z>2$ mm). In the case of Fabry–Peròt straight waveguide lasers the SE nonuniformity is not observed below threshold[14,15] because the cross-section is constant at each position along the resonator axis and the ASE intensity is not intense enough to perturb the carrier distribution. In that case the nonuniformity in the carrier distribution observed above threshold is strictly dependent on the difference between the mirrors reflectivities.[7] Equation (1) has been used to fit the SE intensity curves of Fig. 3(c). The fit gives a logarithmical relation between the net gain and the current [see Fig. 4(a) right axis] in line with that expected for a SQW even though no quantitative information about the gain can be extracted due the high number of unknown quantities and principally the actual value of the intensity.

In the examined laser the clamping of the carrier density does not take place at the lasing threshold, as shown in Fig. 4(a). The SE grows until it begins to saturate between $I=1.2$ A $\approx 1.6 I_{th}$ and $I=1.6$ A. The SE intensity along the longitudinal axis is different but the clamping current range is the same for all regions. At threshold, the total gain of the device is equal to the cavity losses. The total gain has contribution from the gain in RW and tapered sections. In tapered lasers, the photon density is not uniform, being higher in the RW section. Above threshold, the high photon density depletes the carrier density in RW section by stimulated emission and thus saturates the gain in this section. Then the gain in tapered section increases to maintain constant total gain, and this causes the increase in SE observed in the measurements. The *P-I* characteristic, shown in Fig. 4(b), is almost linear with a small change in slope between $I=1.2$ A and $I=1.6$ A corresponding to the transition between the linearly growing SE and the SE saturation.

In conclusion, we have shown that inside a tapered laser the longitudinal carrier density is not uniform below the threshold and that it only fully clamps well above the threshold. The increasing lateral cross-section of the taper induces a nonuniform longitudinal gain distribution to maintain the round-trip gain. This in turn is reflected by a nonuniform longitudinal carrier depletion resulting ultimately in an overall reduction in the device wall plug efficiency. This is an intrinsic characteristic of the device geometry that can be improved by designing the taper with a narrower angle and longer device length permitting a smooth mode expansion and improving the lateral optical mode uniformity.

This work has been supported through the European Union project WWW.BRIGHTER.EU Contract No. IST-2005-035266.

[1] J. N. Walpole, E. S. Kintzer, S. R. Chinn, C. A. Wang, and L. J. Missaggia, Appl. Phys. Lett. **61**, 740 (1992).
[2] J. N. Walpole, Opt. Quantum Electron. **28**, 623 (1996).
[3] F. Dittmar, B. Sumpf, J. Fricke, G. Erbert, and G. Tränkle, IEEE Photon. Technol. Lett. **18**, 601 (2006).
[4] O. B. Jensen, P. E. Andersen, B. Sumpf, K. H. Hasler, G. Erbert, and P. M. Petersen, Proc. SPIE **7582**, 758203 (2010).
[5] M. Spreemann, H. Wenzel, B. Eppich, M. Lichtner, and G. Erbert, IEEE J. Quantum Electron. **47**, 117 (2011).
[6] F. Girardin and G. H. Duan, IEEE J. Sel. Top. Quantum Electron. **3**, 461 (1997).
[7] F. Rinner, J. Rogg, P. Friedmann, M. Mikulla, G. Weimann, and R. Poprawe, Appl. Phys. Lett. **80**, 19 (2002).
[8] F. J. N. Fehr, M. A. Dupertuis, T. P. Hessler, L. Kappei, D. Marti, P. E. Selbmann, B. Deveaud, J. L. Pleumeekers, J. Y. Emery, and B. Dagens, Appl. Phys. Lett. **78**, 4079 (2001).
[9] S. Bull, A. V. Andrianov, J. G. Wykes, J. J. Lim, S. Sujecki, S. C. Auzanneau, M. Calligaro, M. Lecomte, O. Parillaud, M. Krakowski, and E. C. Larkins, IEE Proc.: Optoelectron. **153**, 2 (2006).
[10] L. Borruel, S. Sujecki, P. Moreno, J. Wykes, M. Krakowski, B. Sumpf, P. Sewell, S. C. Auzanneau, H. Wenzel, D. Rodríguez, T. M. Benson, E. C. Larkins, and I. Esquivias, IEEE J. Quantum Electron. **40**, 463 (2004).
[11] M. Krakowski, M. Calligaro, C. Larat, M. Lecomte, N. Michel, O. Parillaud, B. Boulant, and T. Fillardet, Proc. SPIE **5620**, 128 (2004).
[12] A. E. Siegman and R. Arrathoon, IEEE J. Quantum Electron. **3**, 156 (1967).
[13] J. Piprek, *Semiconductor Optoelectronics Devices* (Academic, New York, 2003).
[14] A. J. Bennett, R. D. Clayton, and J. M. Xu, J. Appl. Phys. **83**, 3784 (1998).
[15] E. H. Sargent, D. Pavlidis, H. Anis, N. Golinescu, J. M. Xu, R. Clayton, and H. B. Kim, J. Appl. Phys. **80**, 1904 (1996).